PROCEEDINGS OF SCIENCE

The $B_s \to \mu^+\mu^-\gamma$ decay rate at large q^2 from lattice QCD

R. Frezzotti,[a] **G. Gagliardi,**[b,*] **V. Lubicz,**[b] **G. Martinelli,**[c] **C.T. Sachrajda,**[d] **F. Sanfilippo,**[e] **S. Simula**[e] **and N. Tantalo**[a]

[a] *Dipartimento di Fisica and INFN, Università di Roma "Tor Vergata", Via della Ricerca Scientifica 1, I-00133 Roma, Italy*

[b] *Dipartimento di Fisica, Università Roma Tre and INFN, Sezione di Roma Tre, Via della Vasca Navale 84, I-00146 Rome, Italy*

[c] *Physics Department and INFN Sezione di Roma La Sapienza, Piazzale Aldo Moro 5, 00185 Roma, Italy*

[d] *Department of Physics and Astronomy, University of Southampton, Southampton SO17 1BJ, UK*

[e] *Istituto Nazionale di Fisica Nucleare, Sezione di Roma Tre, Via della Vasca Navale 84, I-00146 Rome, Italy*

We perform a lattice QCD study of the local form factors governing the $B_s \to \mu^+\mu^-\gamma$ decay. To determine the B_s meson form factors, we perform lattice simulations for several values of the heavy-strange meson masses m_{H_s}, within the range $m_{H_s} \in [m_{D_s}, 2m_{D_s}]$, and extrapolate to the physical B_s meson mass, $m_{B_s} \simeq 5.367$ GeV, using heavy quark effective theory (HQET) scaling laws. For this calculation we employ the gauge configurations generated by the ETM Collaboration with $N_f = 2 + 1 + 1$ flavours of Wilson-Clover twisted-mass fermions at maximal twist. We explore the region of large di-muon invariant masses, $\sqrt{q^2} > 4.16\,\text{GeV}$, and use our results to estimate the branching fraction for $B_s \to \mu^+\mu^-\gamma$, recently measured by LHCb in the region $\sqrt{q^2} > 4.9$ GeV.

42nd International Conference on High Energy Physics (ICHEP2024)
18-24 July 2024
Prague, Czech Republic

*Speaker

PoS(ICHEP2024)550

1. Introduction

The flavour-changing neutral current (FCNC) process $B_s \to \mu^+\mu^-\gamma$ is highly suppressed in the Standard Model (SM), making it a promising channel to search for signals of New Physics (NP). Although the LHCb Collaboration has searched for signals of this decay [1, 2], no events have been detected, leading to an upper limit on the branching ratio: $\mathcal{B}(B_s \to \mu^+\mu^-\gamma) < 2.0 \times 10^{-9}$, for photons γ emitted from quarks (initial-state radiation, ISR)[1]. Currently, no first-principles prediction for this decay rate exists. Using lattice QCD, we calculate the form factors F_V, F_A, F_{TV}, F_{TA}, and $\bar{F}_T$, which are the non-perturbative QCD inputs for the determination of the matrix elements $\langle\gamma, \mu^+\mu^-|O_{7,9,10}|\bar{B}s\rangle$.[2] The O_i are the operators in the effective weak Hamiltonian $H_{\rm eff}^{b\to s}$ describing the FCNC $b \to s$ transition. We focus on the large invariant mass region ($\sqrt{q^2} > 4.16$ GeV), where contributions from neglected four-quark and chromomagnetic penguin operators ($O_{1-6,8}$) in $H_{\rm eff}^{b\to s}$ are expected to be small, as they are higher-order in the $1/m_b$ expansion [3]. Among these, charming-penguin diagrams can be important, and we estimate the systematic error induced by our approximation through a phenomenological parameterization of their contribution [4].

Since the $\bar{B}_s$ meson is too heavy for direct simulation on current lattices, we simulate a range of lighter heavy-strange mesons $\bar{H}_s$ (composed of a heavy quark h and a strange anti-quark $\bar{s}$) with masses $m_{H_s} \in [m_{D_s}, 2m_{D_s}]$. Heavy quark effective theory (HQET) relations are then used to guide the extrapolation to the physical $\bar{B}_s$ meson.

2. The effective Hamiltonian and the form factors on the lattice

The low-energy effective weak Hamiltonian describing the $b \to s$ transition, neglecting doubly Cabibbo-suppressed contributions, is given by

$$\mathcal{H}_{\rm eff}^{b\to s} = 2\sqrt{2}G_F V_{tb}V_{ts}^* \left[\sum_{i=1,2} C_i(\mu)O_i^c + \sum_{i=3}^{6} C_i(\mu)O_i + \frac{\alpha_{\rm em}}{4\pi}\sum_{i=7}^{10} C_i(\mu)O_i\right] , \tag{1}$$

where G_F is the Fermi constant, C_i are the Wilson coefficients and O_i are local operators renormalized at the scale μ. With $P_{L(R)} = (1 \mp \gamma^5)/2$, the operators O_i are given by

$$O_1^c = (\bar{s}_i\gamma^\mu P_L c_j)(\bar{c}_j\gamma^\mu P_L b_i) , \qquad O_2^c = (\bar{s}\gamma^\mu P_L c)(\bar{c}\gamma^\mu P_L b) , \tag{2}$$

$$O_7 = -\frac{m_b}{e}\bar{s}\sigma^{\mu\nu}F_{\mu\nu}P_R b , \qquad O_8 = -\frac{g_s m_b}{4\pi\alpha_{\rm em}}\bar{s}\sigma^{\mu\nu}G_{\mu\nu}P_R b , \tag{3}$$

$$O_9 = (\bar{s}\gamma^\mu P_L b)(\bar{\mu}\gamma_\mu\mu) , \qquad O_{10} = (\bar{s}\gamma^\mu P_L b)(\bar{\mu}\gamma_\mu\gamma^5\mu) \tag{4}$$

while O_{3-6} are the QCD penguins. The transition amplitude for the decay is then given by [4]

$$\mathcal{A}[\bar{B}_s \to \mu^+\mu^-\gamma] = -e\frac{\alpha_{\rm em}}{\sqrt{2}\pi}G_F V_{tb}V_{ts}^*\varepsilon_\mu^* \left[\sum_{i=1}^{9} C_i H_i^{\mu\nu}L_{V\nu} + C_{10}\left(H_{10}^{\mu\nu}L_{A\nu} - \frac{i}{2}f_{B_s}L_A^{\mu\nu}p_\nu\right)\right] , \tag{5}$$

where the last term, which depends on the axial decay constant f_{B_s} of the B_s meson, corresponds to the final-state-radiation (FSR) contribution, while the non-perturbative information due to photon emission by the quarks (ISR) is encoded in the hadronic tensors[3] $H_i^{\mu\nu}$, which are pure QCD

[1] The contribution from final-state radiation (FSR), where the photon is emitted from a muon, has been subtracted [1].

[2] The text and figures here and below correspond to the decay of the $\bar{B}_s$ meson.

[3] We refer to our work [4] for the definition of the hadronic tensors $H_i^{\mu\nu}$.

PoS(ICHEP2024)550

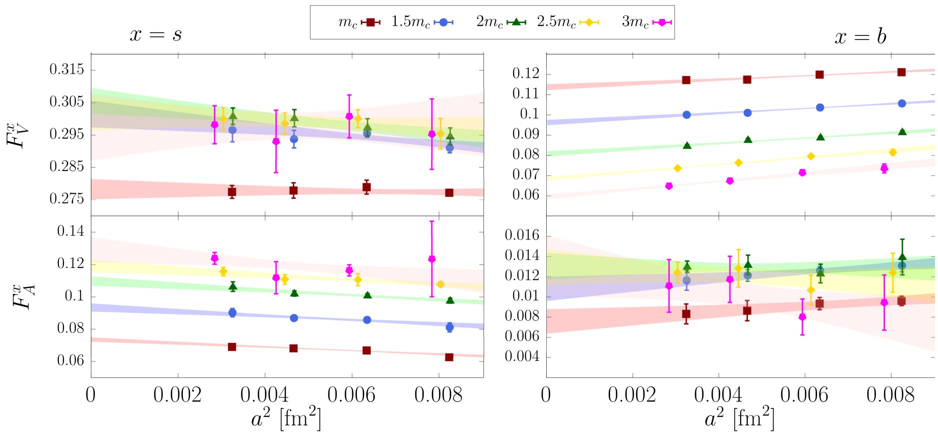

Figure 1: *Continuum-limit extrapolation of the lattice data for the strange- (left panel) and heavy-quark (right panel) contribution to the form factors F_V and F_A for $x_\gamma = 0.4$. The transparent bands correspond to the best-fit function obtained in the linear a^2 fit. In the panels, the different colors correspond to different values of the heavy quark mass m_h.*

quantities. Exploiting Lorentz invariance, the hadronic tensors can be decomposed in terms of form factors. F_V and F_A parameterize the hadronic tensors $H^{\mu\nu}_{9-10}$ corresponding to the semileptonic operators O_{9-10}, while F_{TV}, F_{TA} and $\bar{F}_T$ parameterize $H^{\mu\nu}_7$, which corresponds instead to the contribution of the photon penguin operator O_7. The (local) form factors F_V, F_A, F_{TV}, F_{TA} and $\bar{F}_T$ are functions of the invariant mass $\sqrt{q^2}$ of the $\mu^+\mu^-$ pair, and we find it convenient to express them in terms of the dimensionless variable $x_\gamma = 1 - q^2/m^2_{B_s} = 2E_\gamma/m_{B_s}$, where E_γ is the photon energy in the $\bar{B}_s$-meson rest frame. The simulated values of x_γ are $0.1, 0.2, 0.3, 0.4$. In this proceedings, we discuss the calculation of F_V, F_A, F_{TV} and F_{TA}, which can be determined using standard lattice techniques [4], and provide the dominant contribution to the decay rate. The calculation of the subleading form factor $\bar{F}_T$ is instead more involved and requires the application of recently developed spectral density reconstruction techniques [5]. We refer to our work [4] for further details on the calculation of this contribution.

We compute F_V, F_A, F_{TV}, and F_{TA} using four different $N_f = 2+1+1$ Wilson-Clover twisted mass ensembles, with lattice spacings $a \in [0.056, 0.091]$ fm. This setup, at maximal twist, ensures that the leading discretization errors are proportional to a^2. The form factors are computed for five different values of the heavy-quark mass, specifically $m_h/m_c = 1, 1.5, 2, 2.5, 3$, where m_c is the charm-quark mass. These values of m_h correspond to $m_{H_s} \in [m_{D_s}, 2m_{D_s}]$. Figure 1 shows the lattice-spacing dependence of F_V and F_A for $x_\gamma = 0.4$, distinguishing the contributions from photon emission by the strange and heavy quarks. The bands in the figure correspond to the continuum limit extrapolation that we perform through simple a^2 fits of the data for each value of x_γ and m_h.

Having determined the form factors for $m_{H_s} \in [m_{D_s}, 2m_{D_s}]$, we perform the mass extrapolation to the physical B_s meson mass making use of the scaling laws derived in the framework of the HQET and large-photon-energy expansions [6, 7]. In the effective theory, to leading-order in $1/E_\gamma$ and

$1/m_{H_s}$, the form factors are given by [4]

$$\frac{F_V(x_\gamma, m_{H_s})}{f_{H_s}} = \frac{F_A(x_\gamma, m_{H_s})}{f_{H_s}} = \frac{|q_s|}{x_\gamma}\frac{R(E_\gamma,\mu)}{\lambda_B(\mu)} \tag{6}$$

$$\frac{F_{TV}(x_\gamma, m_{H_s},\mu)}{f_{H_s}} = \frac{F_{TA}(x_\gamma, m_{H_s},\mu)}{f_{H_s}} = \frac{|q_s|}{x_\gamma}\frac{R_T(E_\gamma,\mu)}{\lambda_B(\mu)}\,, \tag{7}$$

where q_s is the electric charge of the strange quark, λ_B is the first inverse moment of the B_s-meson light-cone distribution amplitude, and R and R_T are radiative correction factors [6]. f_{H_s} is instead the axial decay constant of the $\bar{H}_s$ meson, which we determine non-perturbatively. In the large mass/energy effective theory, the leading contribution comes from the photon emitted by the strange-quark, while the emission from the heavy-quark is suppressed by an additional power of $1/m_{H_s}$. The relations above, being valid for large E_γ (i.e. for small q^2), are however insufficient to describe the behaviour of the form factors in the range of simulated x_γ and m_{H_s}, due to sizable resonance contributions which give rise to the following modification of the previous LO relations [4]

$$\frac{F_V(x_\gamma, m_{H_s})}{f_{H_s}} = \frac{|q_s|}{x_\gamma + \frac{2C_V}{m^2_{H_s}}}\frac{R(E_\gamma,\mu)}{\lambda_B(\mu)}\,, \qquad \frac{F_A(x_\gamma, m_{H_s})}{f_{H_s}} = \frac{|q_s|}{x_\gamma + \frac{2C_A}{m_{H_s}}}\frac{R(E_\gamma,\mu)}{\lambda_B(\mu)}\,, \tag{8}$$

where, within the vector-meson-dominance (VMD) approximation, the pole parameters C_A and C_V are related to the mass splitting between the $\bar{H}_s$ pseudoscalar meson and the ground-state vector ($\bar{H}_s^*$) and axial-vector ($\bar{H}_{s1}$) mesons via

$$C_V = \frac{m^2_{H_s^*} - m^2_{H_s}}{2} \simeq (0.5\ \text{GeV})^2\,, \qquad C_A = m_{H_{s1}} - m_{H_s} \simeq 0.5\ \text{GeV}\,. \tag{9}$$

Similar relations hold for F_{TV} and F_{TA} too [4]. We perform the extrapolation to the physical B_s-meson point through a simultaneous global fit of the mass and x_γ dependence of all four form factors, employing a fit Ansatz which includes the resonance corrections in Eq. (8), as well as the NLO and NNLO corrections of order $O(\frac{1}{E_\gamma}, \frac{1}{m_{H_s}})$ and $O(\frac{1}{E_\gamma^2}, \frac{1}{m^2_{H_s}})$ to the LO relations in Eq. (6). The full fit Ansatz is thoroughly discussed in [4], to which we refer for further technical details. The results of the combined fits are shown in Figure 2, where the bands correspond to the best-fit functions, and the vertical line to the physical point $m_{H_s} = m_{B_s}$. The pole terms nicely describe the behaviour of the form factors at small x_γ (where they are more relevant), and we obtain for C_V and C_A, which are free-parameters in our fits, the values $C_V^{\text{fit}} = (0.57(3)\ \text{GeV})^2$ and $C_A^{\text{fit}} = 0.70(7)$ GeV, which although slightly larger than the values in Eq. (9), are in line with the expectations from VMD. In Figure 3, we compare our results for the form factors at the physical point with existing determinations based on light-cone sum rules [8], on the relativistic dispersion approach based on the constituent-quark picture [9], and on a hybrid approach [10] which uses lattice QCD results for $D_s \to \ell\nu_\ell\gamma$ in combination with quark-model and VMD-inspired relations, to infer the vector and axial-vector form factors of $B_s \to \mu\mu\gamma$. As the figure shows, with a few exceptions, our results differ significantly from the earlier estimates, which in turn disagree with each other. In particular our results are smaller than the light-cone sum rule predictions [8], and larger than both the quark-model results [9] and those of the hybrid approach [10].

[4] For the tensor form factors we have explicitly inserted in the l.h.s. the dependence on the renormalization scale μ, which is instead absent in F_V and F_A which are scale-independent quantities. In the following, our results for F_{TV} and F_{TA} are given in the $\overline{MS}$ scheme at the scale $\mu = 5$ GeV.

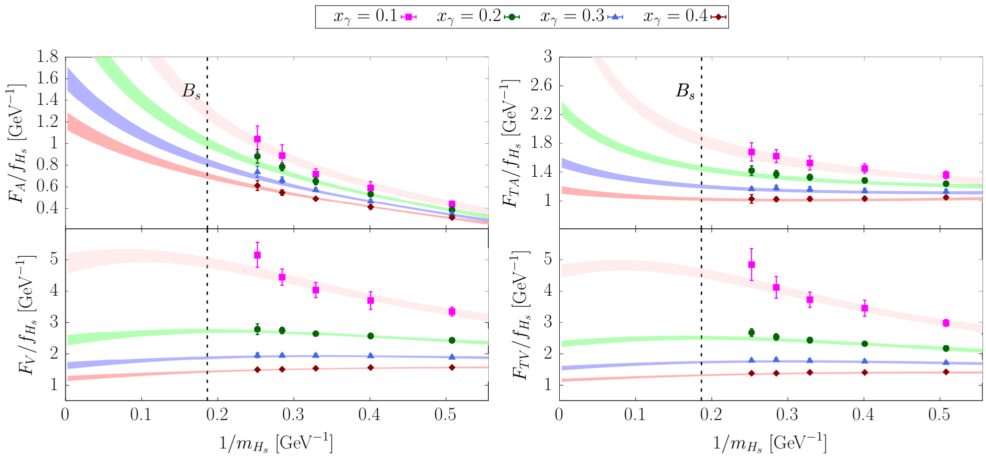

Figure 2: *Extrapolation to the physical B_s meson of the four form factors F_A (top left) , F_{TA} (top right), F_V (bottom left) and F_{TV} (bottom right). The different colors correspond to the different simulated values of x_γ. The continuum bands correspond to the best-fit function obtained in the mass-extrapolation fits.*

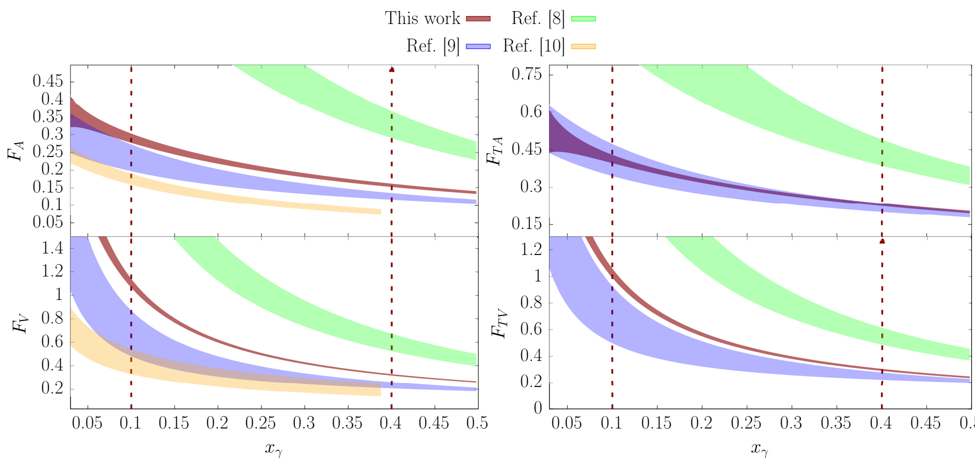

Figure 3: *Comparison between our results for the form factors (red bands), and existing model-dependent results [8–10]. The region between the vertical red dashed lines corresponds to the region of simulated x_γ, and therefore within this region our results are obtained through an interpolation of our lattice data.*

3. Results for the branching fractions

We use our form factor results to evaluate the ISR contribution to the branching fractions

$$\mathcal{B}_{\rm SD}(x_\gamma^{\rm cut}) = \int_0^{x_\gamma^{\rm cut}} {\rm d}x_\gamma \, \frac{{\rm d}\mathcal{B}_{\rm SD}}{{\rm d}x_\gamma} \,, \tag{10}$$

where $E_\gamma^{\rm cut} = m_{B_s} x_\gamma^{\rm cut}/2$ is the upper photon energy limit, and ${\rm d}\mathcal{B}_{\rm SD}/{\rm d}x_\gamma$ is the ISR contribution to the differential branching fraction[5]. The left panel of Figure 4 shows our results, with the red band representing the branching fractions calculated neglecting four-quark and chromomagnetic penguin contributions. As already mentioned, these contributions are expected to be small for low $x_\gamma^{\rm cut}$. However, to estimate the associated systematic error, we included a phenomenological description

[5] The interference between ISR and FSR contributions is negligible for all $x_\gamma^{\rm cut}$ [4].

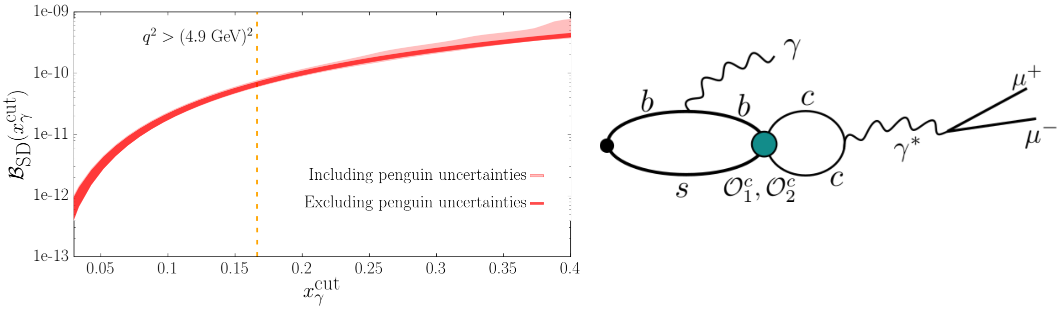

Figure 4: *Left: Our determination of the ISR contribution $\mathcal{B}_{\rm SD}(x_\gamma^{\rm cut})$. The red and light-red bands differ on whether $\Delta C_9(q^2)$ in Eq. (11) has been included or not, while the vertical line corresponds to the experimental cut imposed by the LHCb Collaboration [1, 2]. Right: charming-penguin diagram due to the four-quarks operators O^c_{1-2} (the corresponding diagram with the real photon emitted from the strange quark is not shown).*

of the charming-penguin diagram (right panel of Figure 4), which likely dominates the neglected contributions due to the presence of broad $c\bar{c}$ resonances near or within the q^2 region we explored. Following previous works [3, 9, 10], we account for this contribution by introducing a q^2-dependent shift to the Wilson coefficient C_9: $C_9 \to C_9^{\rm eff}(q^2) = C_9 + \Delta C_9(q^2)$. The shift $\Delta C_9(q^2)$ is modeled as a sum over $J^P = 1^-$ charmonium resonances [9, 10]:

$$\Delta C_9(q^2) = -\frac{9\pi}{\alpha_{\rm em}^2}(C_1 + \frac{C_2}{3}), \sum_V |k_V| e^{i\delta_V} \frac{m_V B(V \to \mu^+\mu^-)\Gamma_V}{q^2 - m_V^2 + i m_V \Gamma_V}\,, \tag{11}$$

where Γ_V, m_V, and $B(V \to \mu^+\mu^-)$ represent the resonance's total decay width, mass, and branching fraction into $\mu^+\mu^-$. For the lowest resonances, these values come from experiments, but little is known about phase shifts δ_V and fudge factors k_V. To be conservative, we assume the phases are uniformly distributed in $[0, 2\pi)$ and use $k_V = 1.75 \pm 0.75$. Including ΔC_9 produces the light-red band in Figure 4 (left panel), representing our final result. Charming-penguin uncertainties dominate for $x_\gamma^{\rm cut} > 0.2$, necessitating a first-principles calculation to improve the predictions of $\mathcal{B}_{\rm SD}(x_\gamma^{\rm cut})$ in this region. At $x_\gamma^{\rm cut} \simeq 0.166$ (indicated in the left panel of Figure 4 by the vertical dashed line) we can compare our result $\mathcal{B}_{\rm SD}(0.166) = 6.9(9) \times 10^{-11}$ with the LHCb upper-bound [1, 2], $\mathcal{B}_{\rm SD}^{\rm LHCb}(0.166) < 2 \times 10^{-9}$, which is more than one order of magnitude larger than our result [6].

References

[1] R. Aaij *et al.* [LHCb], Phys. Rev. D **105** (2022) no.1, 012010.
[2] R. Aaij *et al.* [LHCb], Phys. Rev. Lett. **128** (2022) no.4, 041801.
[3] D. Guadagnoli, M. Reboud and R. Zwicky, JHEP **11** (2017), 184.
[4] R. Frezzotti *et al.* Phys. Rev. D **109** (2024) no.11, 114506.
[5] R. Frezzotti *et al.* Phys. Rev. D **108** (2023) no.7, 074510.
[6] M. Beneke and J. Rohrwild, Eur. Phys. J. C **71** (2011), 1818.
[7] M. Beneke, C. Bobeth and Y. M. Wang, JHEP **12** (2020), 148.
[8] T. Janowski, B. Pullin and R. Zwicky, JHEP **12** (2021), 008.
[9] A. Kozachuk, D. Melikhov and N. Nikitin, Phys. Rev. D **97** (2018) no.5, 053007.
[10] D. Guadagnoli, C. Normand, S. Simula and L. Vittorio, JHEP **07** (2023), 112.
[11] R. Aaij *et al.* [LHCb], JHEP **07** (2024), 101.

[6] Recently, the LHCb Collaboration has presented a new upper bound based on an analysis with explicit detection of the final state photon [11]. Above the $c\bar{c}$ resonances, the bound is however weaker than the earlier result [1, 2].